nature communications

Article

https://doi.org/10.1038/s41467-024-51540-1

Microporous membrane with ionized sub-nanochannels enabling highly selective monovalent and divalent anion separation

Received: 30 May 2024

Accepted: 9 August 2024

Published online: 23 August 2024

Check for updates

Mei-Ling Liu[1,2,5], Yu Chen[1,5], Chuan Hu[3], Chun-Xu Zhang[1], Zheng-Jun Fu[1], Zhijun Xu[1], Young Moo Lee[3] ✉ & Shi-Peng Sun[1,2,4] ✉

Membranes tailored for selective ion transport represent a promising avenue toward enhancing sustainability across various fields including water treatment, resource recovery, and energy conversion and storage. While nanochannels formed by polymers of intrinsic microporosity (PIM) offer a compelling solution with their uniform and durable nanometer-sized pores, their effectiveness is hindered by limited interactions between ions and nanochannel. Herein, we introduce the randomly twisted V-shaped structure of Tröger's Base unit and quaternary ammonium groups to construct ionized sub-nanochannel with a window size of 5.89–6.54 Å between anion hydration and Stokes diameter, which enhanced the dehydrated monovalent ion transport. Combining the size sieving and electrostatic interaction effects, sub-nanochannel membranes achieved exceptional ion selectivity of 106 for Cl^-/CO_3^{2-} and 82 for Cl^-/SO_4^{2-}, significantly surpassing the state-of-the-art membranes. This work provides an efficient template for creating functionalized sub-nanometer channels in PIM membranes, and paves the way for the development of precise ion separation applications.

Rapid industrialization, accompanied by excessive carbon emissions, exacerbates global warming and imposes substantial and significant pressure on energy security[1–3]. Efficiently recovering carbon-containing substances and transforming them into valuable products could substantially mitigate carbon emissions and pollution[4,5]. For instance, converting carbon-containing organic compounds or carbon dioxide into carbonates offers an ideal pathway for their reuse and recycling, necessitating efficient separations of carbonates from other species[6]. Among these, the separation between carbonate and chloride ions is particularly significant in various applications, including heavy metal extraction[7], antibiotic degradation[8], and the production of battery-grade carbonates such as lithium carbonate and sodium carbonate. Membrane-based separation processes offer a promising avenue for such separations of similar molecules, relying on the development of selective transport channels[9–11]. However, the similar radii and physical properties of these coexisting ions with carbonates complicates the separation of these ions[12]. Therefore, research has rarely been reported on the separation and extraction of carbonate with other similar ions.

As the pore size of the channels in the membranes can be confined to the sub-nanometer scale, enhanced membrane-ion interactions such as friction and slip flow can effectively improve the selectivity of monovalent and divalent ions, which is promising for more accurate separation of specific ions[13,14]. In addition, an electric field is a powerful tool to offer ions an external driving force and promote their directional migration[15]. Using the movement direction of the electric field can facilitate the mobility of ions in nanochannels and increase ion transport. During the electric driving process, the properties of the

[1]State Key Laboratories of Materials-Oriented Chemical Engineering, National Engineering Research Center for Special Separation Membranes, College of Chemical Engineering, Nanjing Tech University, Nanjing 211816, China. [2]NJTECH University Suzhou Future Membrane Technology Innovation Center, Suzhou 215100, China. [3]Department of Energy Engineering, College of Engineering, Hanyang University, Seoul 04763, Republic of Korea. [4]Suzhou Laboratory, Suzhou 215100, China. [5]These authors contributed equally: Mei-Ling Liu, Yu Chen. ✉e-mail: ymlee@hanyang.ac.kr; ssp@njtech.edu.cn

anion exchange membrane (AEM) are crucial for anion transport and separation efficiency[16]. Numerous materials based on cationic groups, such as quaternary ammonium (QA), have been investigated to form ion-conducting regions via microphase separation to facilitate anion diffusion[17]. However, traditional polymers have mostly flexible structures with a wide range of pore size distributions. Moreover, the flexible polymer backbone swells easily and collapses the membrane pores, resulting in poor separation selectivity and stability, especially in electrochemical processes.

Polymers of intrinsic microporosity (PIM) with shape-persistent units show high rigidity to prevent free rotation of the main chain[18,19]. Their inefficiently stacked molecular chains can produce randomly twisted nanochannels (pore size < 2 nm), which possess a high free volume fraction to facilitate the diffusion of molecules[20,21]. Among them, a polymer of Tröger's Base (TB) that contains a rigid V structure imparted by a methano[1,5]diazocine bridge is a typical example[22,23]. The key TB units can make available the sub-nanometer microporosities between distorted polymer chains, which are expected for highly efficient transport of special ions and alkaline stability combined with inhibition of membrane swelling[24]. However, the absence of ion-interacting groups within the sub-nanochannel increases the energy barrier of anion entry, resulting in a reciprocal relationship between anion selectivity and conductivity.

Herein, quaternary ammonium-functionalized TB microporous polymer membranes with sub-nanochannels were well-designed for ion separations. The quaternization process reduces the pore size distribution of the microporous membrane to the range of 5.89–6.54 Å, which is smaller than the hydration diameters of Cl^-, CO_3^{2-}, and SO_4^{2-} (Fig. 1). In addition, the introduction of QA groups (with a positive charge) to the polymer backbone facilitated the formation of microphase separation structures and provided channels for dehydrated ion transport. Meanwhile, the differences in the dehydration energies of anions and their adsorption and desorption energies on the QA-TB framework could cause different rates of ion mobility, increasing ion separation. As expected, the excellent separation performance between monovalent and divalent anions and high chemical stability in 12 day continuous ion separation experiments are exhibited. This may provide a material design strategy for existing ion separation technologies and significantly improve separation efficiency.

Results

Tailoring TB polymers with QA groups for enhanced membrane properties

As depicted in Fig. 2a, the TB polymers were synthesized from o-benzidine (DMB) and dimethoxymethane (DMM) monomers via an acid-catalyzed polycondensation reaction[25], as verified by Fourier-transform infrared spectra and ^{1}H nuclear magnetic resonance (Supplementary Figs. 1–2). The QA groups were then incorporated into the TB polymer skeleton to provide an ion transport channel (Supplementary Fig. 3-4). The structural composition of the TB units and the incorporation of QA groups give TB/QA-TB membranes distinctive and superior physical and chemical properties. The membranes have the characteristic surface of dense polymer membranes without obvious defects (Supplementary Fig. 5). As shown in Fig. 2b, dynamic mechanical analysis (DMA) was employed to probe the thermal resilience of the membranes. Both TB and QA-TB membranes exhibited a remarkable storage modulus exceeding 1000 MPa within the temperature range of 120 to 290 °C, showcasing outstanding thermo-mechanical stability. Additionally, tensile strength plays a pivotal role in membrane performance and mechanical stability. Given the high rigidity of PIM materials, both membranes demonstrated substantial tensile strength of ~60 MPa (Supplementary Fig. 6). Moreover, TB polymers with rigid backbones and pronounced hydrophobic characteristics are effective in mitigating membrane swelling. As a result, TB and QA-TB membranes exhibited low water uptake values of 4.05% and 1.75%, respectively, accompanied by corresponding swelling ratios of 0.99% and 1.01% (Fig. 2c). The swelling ratios for both TB and QA-TB membranes were significantly lower at room temperature compared with other ion exchange membranes in the literature (Supplementary Table 1).

Polymer membranes designed for ion separation commonly necessitate a high ion exchange capacity (IEC) to ensure superior ionic

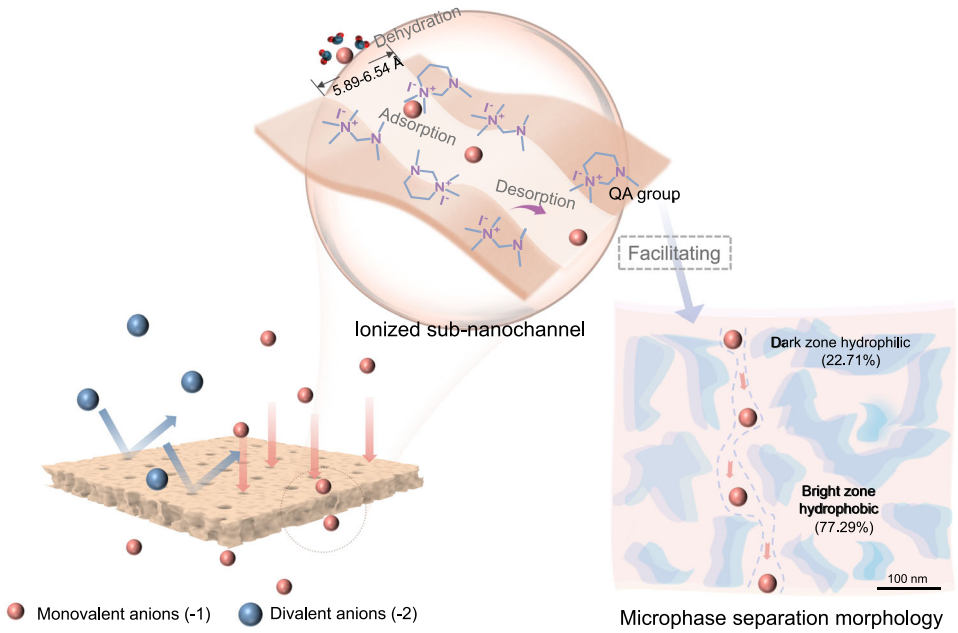

Fig. 1 | Schematic illustration of the Tröger's Base (TB) microporous polymer membrane for ion separations. Ionized sub-nanochannels were engineered through the strategic integration of angstrom-porous quaternized TB units with ion adsorption sites. The randomly twisted V-shaped structure of TB provides regulated membrane pores with a pore window size of 5.89–6.54 Å, positioned between the anion hydration diameter and their Stokes diameter. Additionally, the incorporation of functional groups (quaternary ammonium groups) promoted channel-ion interactions and improved the monovalent ion flux.

https://doi.org/10.1038/s41467-024-51540-1

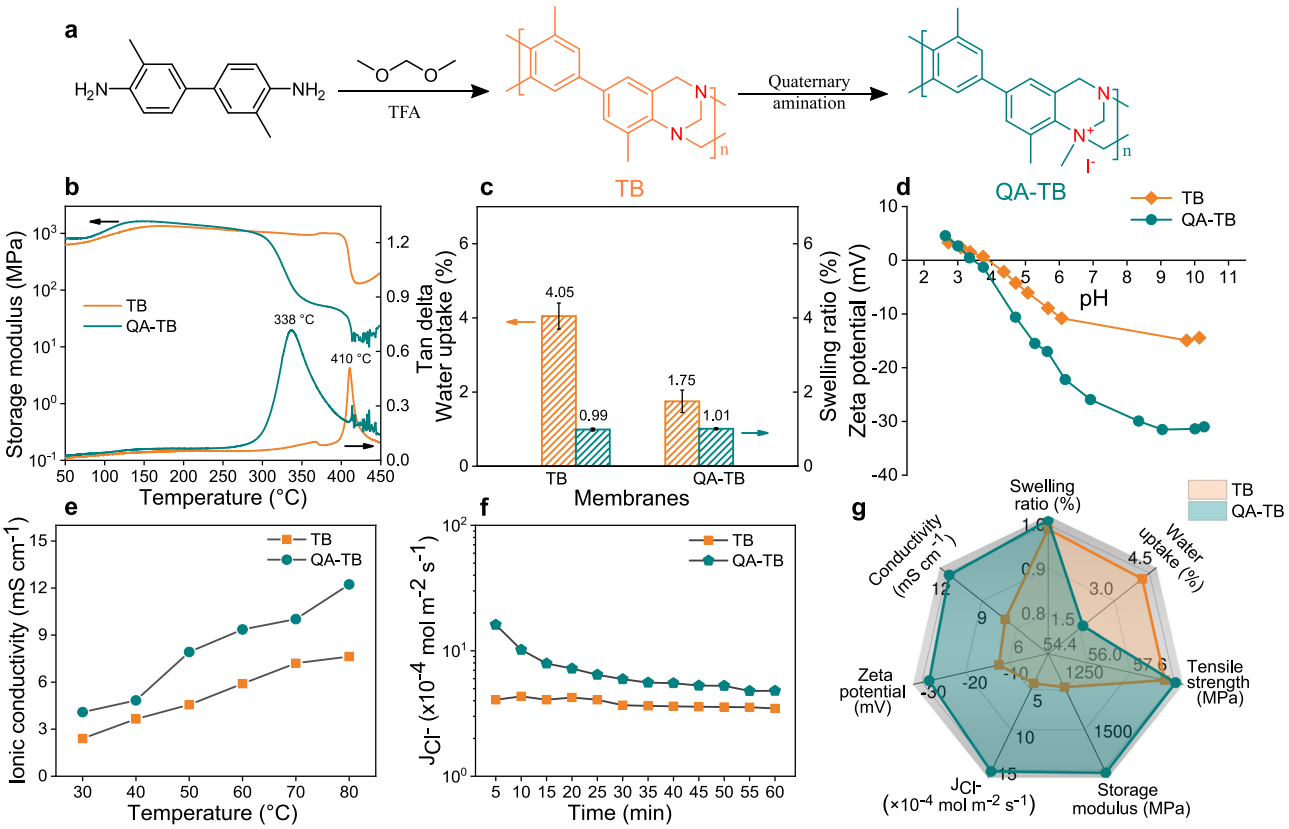

Fig. 2 | Synthesis routes and physicochemical properties of TB and QA-TB membranes. a Synthetic pathway for TB and QA-TB polymers. **b** Thermo-mechanical analysis, (**c**) water uptake and swelling ratios, (**d**) zeta potential curves, (**e**) ionic conductivity, and (**f**) ion fluxes of TB and QA-TB membranes. Error bars represent the standard deviation calculated from three parallel measurements. **g** Radar plot comparing the physicochemical properties of TB and QA-TB membranes.

conductivity and effective ion separation within the designated channels. Nonetheless, the high IEC of a membrane often accompanies increased water retention, resulting in substantial swelling ratios that may jeopardize the integrated structure and stable performance of the membranes[26]. Remarkably, in this work, the QA-TB membranes exhibited significantly lower swelling ratios while the IEC remained at a mere 0.0167 meq g^{-1}. This minimal value is ascribed to a strong adsorption force of I^- within the membrane, hindering its release during the ion exchange process. As illustrated by the zeta potential spectra in Fig. 2d, the QA-TB membrane exhibited a more pronounced negative charge, which could be attributed to the presence of absorbed I^-. However, the introduction of charged QA groups effectively increases the ionic conductivity of QA-TB membrane (Fig. 2e). Moreover, the QA-TB membrane demonstrates a notably elevated monovalent anion flux, surpassing that of the TB membrane to a significant degree (Fig. 2f). This indicates that, despite the decrease in IEC value of the QA-TB membrane, the engineered ionized sub-nanochannels remain capable of ensuring smooth transport of monovalent anions. A comparison of the membrane properties (Fig. 2g and Supplementary Table 2) indicates that the QA-TB membrane is more adept at facilitating the migration of monovalent ions, rendering it better suited for the separation of monovalent and divalent anions.

Probing Cl^- and CO_3^{2-} ion migration

To evaluate the selectivity of the QA-TB membrane toward monovalent and divalent anions, an electrochemical device comprised of four compartments was employed. The effective area of the membrane inside the device was 19.63 cm^2. Considering the optimal performance on targeted ion flux and selectivity, the following conditions were employed in the subsequent ion separation experiments: an ion concentration of 100 mM, a concentration chamber to dilution chamber volume ratio of 1:1, and a current density of 100 A m^{-2} (Fig. 3a). This approach exhibits low energy consumption in different systems, with an energy consumption ratio of ~0.42–0.48 kWh·mol^{-1}, and maintains a current efficiency above 60% even after the continuous 24 h operation (Supplementary Fig. 7).

The migration of Cl^- and CO_3^{2-} anions in 1 h was examined, as in Fig. 3b, c. Initially, Cl^- was preferentially transported across the membrane within the initial 25 min and exhibited an increase in migration amount over time. Intriguingly, there was no discernible migration of CO_3^{2-} during this period. Although a minimal migration of CO_3^{2-} was observed within the final 35 min, amounting to less than one-fifth of the migration of Cl^-, it remained relatively steady (Fig. 3b). Because CO_3^{2-} exhibits greater dehydration difficulty and consequently migrates more slowly than Cl^- ions, especially when hydrated. Furthermore, the ion flux data visually indicated the preferential migration of Cl^-. The Cl^- flux peaked at 16.13×10^{-4} mol m^{-2} s^{-1}, and the subsequent decrease (Fig. 3c) could be ascribed to the continuous reduction in the overall concentration of Cl^- inside the dilution chamber. In addition, CO_3^{2-} readily undergoes hydrolysis, producing a small amount of HCO_3^- that may compete with Cl^- and decrease the migration rate of Cl^-. The *pH* value of the solution could influence the hydrolysis degree and the existing form of CO_3^{2-} [27]. To mitigate the influence of HCO_3^- on the separation process, the *pH* value of the solution was monitored while titrating the concentration of CO_3^{2-}. No substantial alterations in *pH* and CO_3^{2-} were found in the dilution chamber, indicating that CO_3^{2-} remained the predominant form in the solution (Supplementary Fig. 8). Consequently, only a minimal amount of CO_3^{2-} underwent hydrolysis, allowing a negligible portion to

https://doi.org/10.1038/s41467-024-51540-1

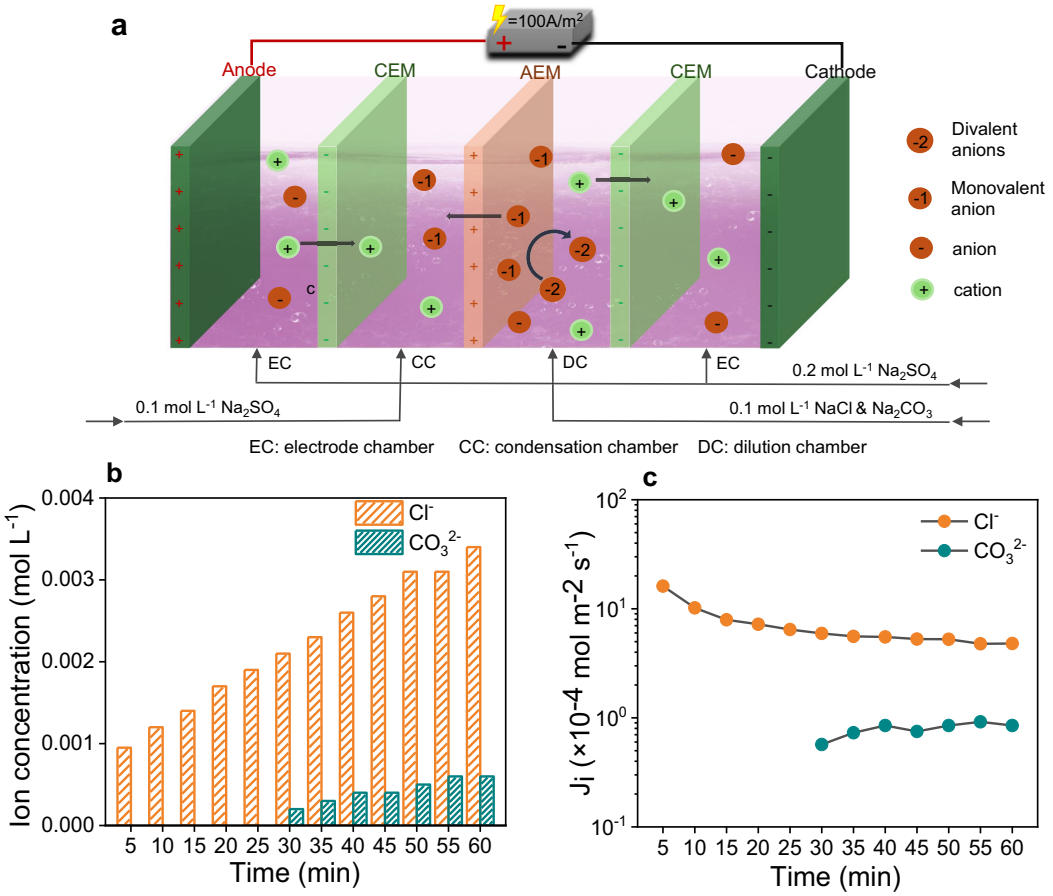

Fig. 3 | Short-term migration of Cl^- and CO_3^{2-} anions. a Schematic diagram of the four-compartment electrochemical device for ion separation. The CEMs were SPEEK membranes and the AEMs were QA-TB membranes. **b** Concentration profiles in the concentration chamber and (**c**) ion fluxes of Cl^- and CO_3^{2-} through the QA-TB membrane during the 1-h experiment.

migrate. This circumstance of different migration rates enhances the selectivity of the separation between the two ions.

Sustained separation of Cl^- and CO_3^{2-}

The sub-nanochannels in the QA-TB membrane demonstrated a remarkable ability to promote the migration of monovalent anions and limit the transport of divalent anions (Fig. 4a). To investigate the long-term separation performance of the membrane, the QA-TB membrane was tested for 12 consecutive days to monitor the ion flux and permeation selectivity. As depicted in Fig. 4b, although the ion flux gradually decreased over time, the Cl^- flux remained significantly higher than that of CO_3^{2-} by an order of magnitude. As a result, the migration amount of Cl^- in the concentration chamber steadily increased over 12 days until it plateaued due to complete migration of Cl^- in the dilution chamber, whereas the slow penetration of CO_3^{2-} resulted in its migration remaining minimal and plateaued (Fig. 4c). Consequently, the concentrations of the two ions in the concentration chamber exhibited a tenfold difference, effectively elevating the permeation selectivity to 106 (Fig. 4d).

Expanding applicability: Cl^-/SO_4^{2-} separation and literature comparison

While the separation of Cl^- and CO_3^{2-} showcased the exceptional selectivity of the QA-TB membrane for monovalent/divalent anion pairs, studies on this specific separation are relatively scarce in the literature. To facilitate a more comprehensive evaluation and direct comparison with established benchmarks, we investigated the performance of the QA-TB membrane for separating Cl^- from another commonly encountered divalent anion, sulfate (SO_4^{2-}). Industries like petroleum, pharmaceutical plants, and paper mills often produce vast amounts of highly saline wastewater containing sulfates and chlorides[28,29]. Consequently, the separation of Cl^- and SO_4^{2-} is crucial. During Cl^-/SO_4^{2-} separation trials, the QA-TB membrane demonstrated outstanding separation efficiency. The migration of Cl^- in 1 h was markedly higher than that of SO_4^{2-} (Supplementary Fig. 9), achieving a Cl^- flux of 20.37×10^{-4} mol m^{-2} s^{-1} and a permeation selectivity of 82 (Supplementary Fig. 10). The ion migration rate was even faster than that in the Cl^-/CO_3^{2-} system, with complete Cl^- migration achieved within 48 h (Supplementary Fig. 11), while the optimal permeation selectivity was slightly lower ($P_{SO_4^{2-}}^{Cl^-} = 82 < P_{CO_3^{2-}}^{Cl^-} = 106$). This difference arises from that a small amount of HCO_3^- initially reduces the Cl^- flux, while CO_3^{2-} has larger size and higher hydration free energy compared to Cl^- and SO_4^{2-}. Consequently, CO_3^{2-} dehydrates and migrates at the slowest rate, resulting in higher selectivity for separation from Cl^-. However, the Cl^- and SO_4^{2-} separation performance of the QA-TB membrane far exceeds those reported in the literature (Fig. 4e and Supplementary Table 3).

Unveiling separation mechanisms: ion dehydration, microphase separation, and ion interactions

The excellent selectivity of the QA-TB membrane for monovalent and divalent anions could stem from the size effect and the presence of the induced QA groups. On the one hand, the constructed ion channels are

https://doi.org/10.1038/s41467-024-51540-1

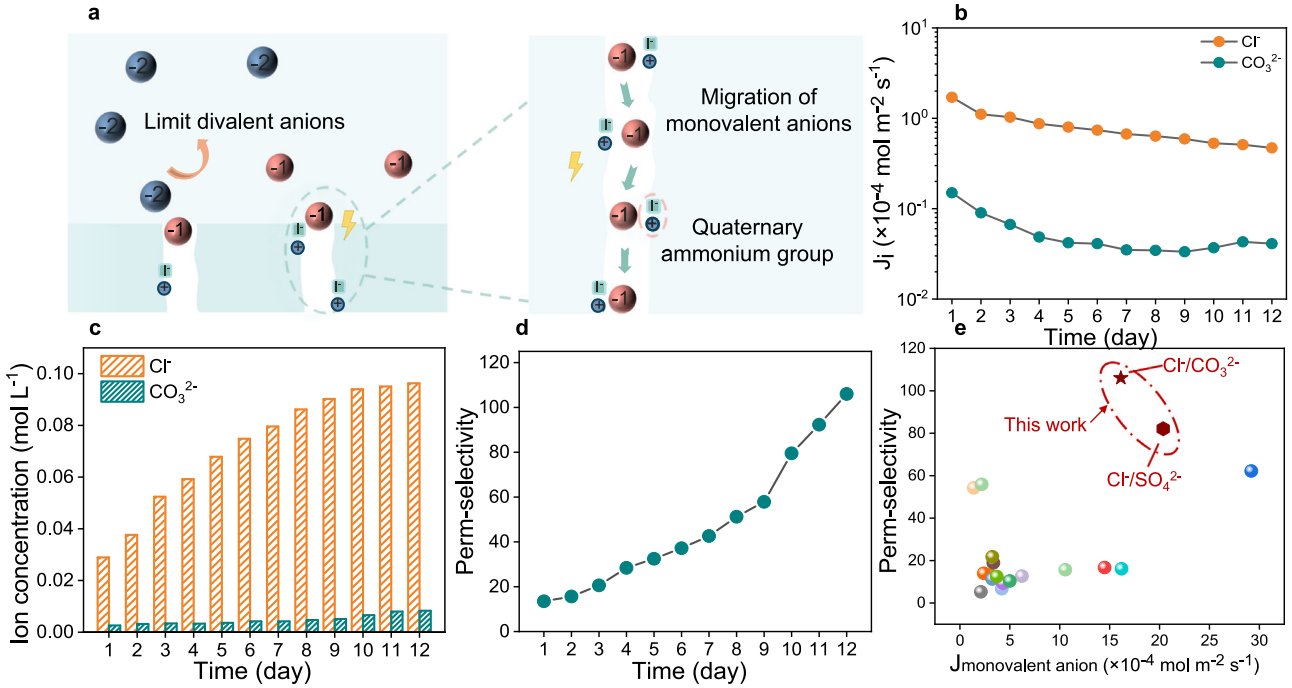

Fig. 4 | Long-term separation performance of the QA-TB membrane for monovalent and divalent anions. a Schematic illustration depicting the promotion of monovalent anion migration and limitation of divalent anion transport through the sub-nanochannels of the QA-TB membrane. **b** Comparison of monovalent and divalent ion fluxes over 12 days. **c** Ion concentration in the concentration chamber. **d** Perm-selectivity of the QA-TB membrane for Cl^- and CO_3^{2-} separation. **e** Comparison of monovalent and divalent anion separation performance of QA-TB membrane with previously reported membranes.

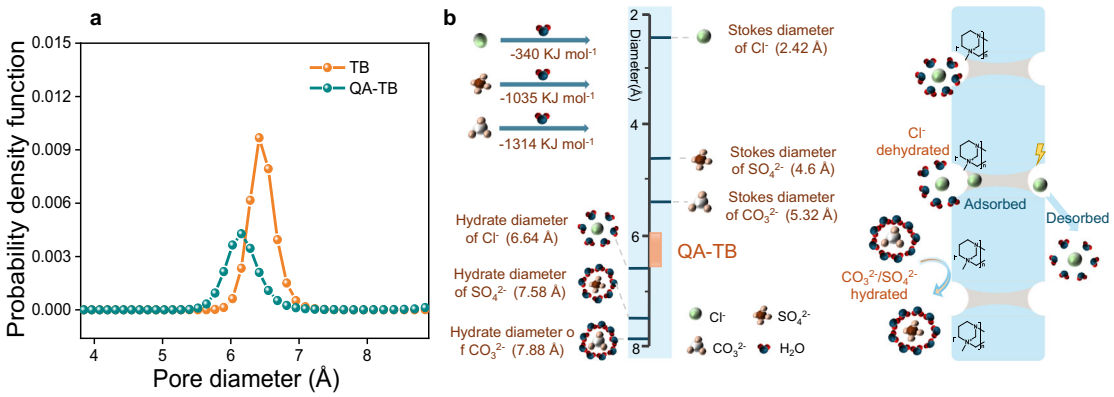

Fig. 5 | Effect of pore size of microporous membranes on the separation performance for differentiating monovalent and divalent anions. a Free volume pore sizes of the TB and QA-TB membranes obtained via PALS. **b** Schematic illustration of the separation mechanisms for monovalent (Cl^-) and divalent (CO_3^{2-}, SO_4^{2-}) anions, considering the influence of hydration energy.

unable to accommodate the migration of hydrated ions, resulting in dehydration. The dehydration ability of ions directly influences their diffusion speed through sub-nanochannels[30]. On the other hand, the distinct hydrophilic and hydrophobic properties between the polymer backbone and the introduced QA groups facilitate the formation of a microphase separation structure within the membrane, which provides channels for the migration of ions[31]. Meanwhile, different degrees of electrostatic interaction between the QA-TB framework and ions help ions with different free energies and transfer along the pore walls at different speeds. Greater disparity in migration rates could lead to higher selectivity in the separation process.

Appropriate characterizations were conducted to support this mechanism. First, the dense nature of the material impedes the smooth migration of hydrated ions through the constructed ion channels based on the size sieving effect. The microporosity of the membranes was characterized using positron annihilation lifetime spectroscopy (PALS). As depicted in Supplementary Figs. 12–13 and Fig. 5a, the pore size of the QA-TB membrane is smaller than that of the TB membrane, which can be attributed to quaternization enhancing ionic/polar chain interactions[32]. Therefore, the fractional free volume (FFV) decreased, and the membrane cavities were reduced (Supplementary Table 4). In Fig. 5b and Supplementary Table 5, a comparison of the ion sizes reveals significant differences between bare ions and hydrated ions, with the pore size of the QA-TB membrane falling between their hydration diameter and the Stokes diameter. Additionally, significantly different hydration free energies are observed for Cl^-, CO_3^{2-}, and SO_4^{2-}. The minimal hydration-free energy of Cl^- eases the shedding of the surrounding H_2O molecules. However, SO_4^{2-} and CO_3^{2-}

https://doi.org/10.1038/s41467-024-51540-1

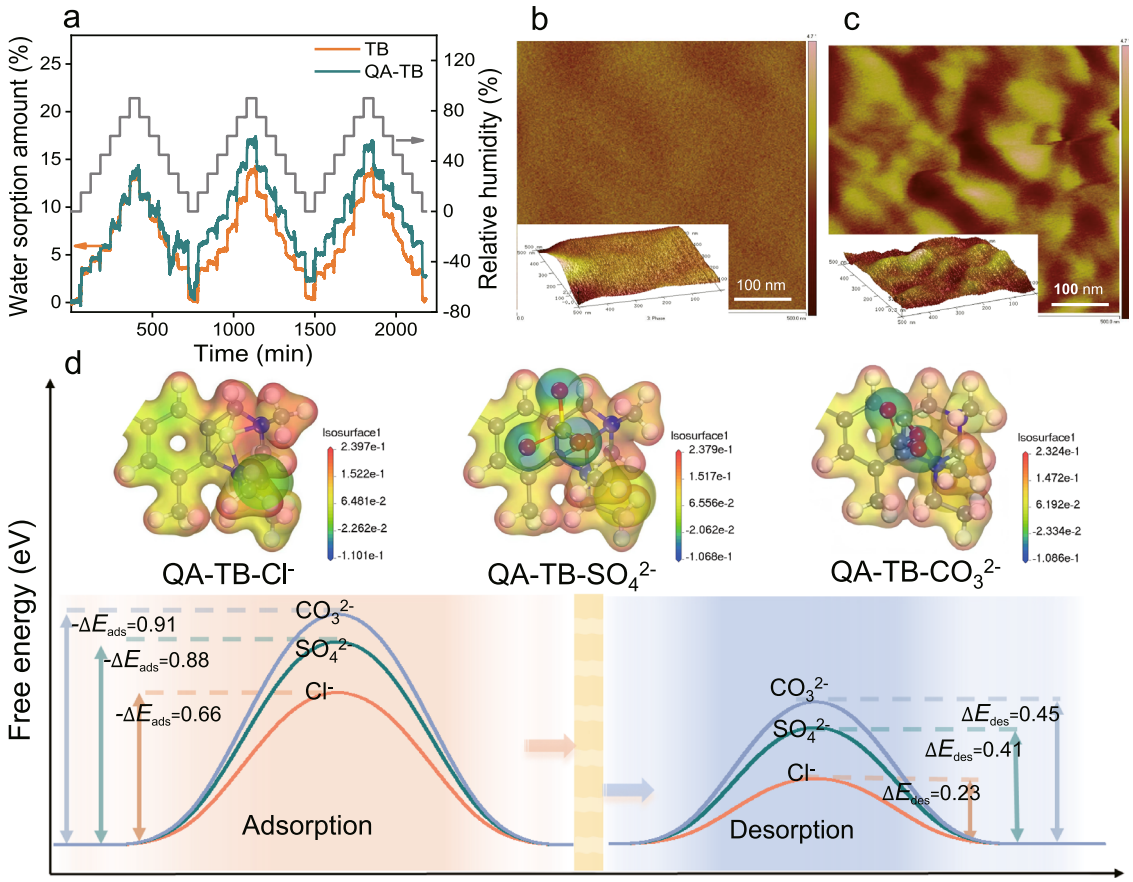

Fig. 6 | Anion separation across the ionized sub-nanochannels. a Water sorption behavior of TB and QA-TB membranes investigated using dynamic vapor sorption (DVS). Atomic force microscopy (AFM) images of the (**b**) TB membrane and (**c**) QA-TB membrane. The bright regions in (**c**) represent the hydrophobic segments of the polymer backbone, whereas the dark regions correspond to the hydrophilic portions of the QA groups. The partitioning calculation using ImageJ software reveals that the percentage of hydrophilic region is about 22.71% and the percentage of hydrophobic region is about 77.29%. **d** Electrostatic potential diagrams and calculations of adsorption and desorption energies for $Cl^-/SO_4^{2-}/CO_3^{2-}$ on the surface of QA-TB. The CO_3^{2-} exhibits greater negative adsorption energy, indicating stronger adsorption to QA-TB, and has higher desorption energy, hindering desorption. Conversely, Cl^- shows the lowest free energy, resulting in faster migration.

possess considerably higher hydration free energies and form stronger bonds with water molecules[33]. In particular, CO_3^{2-} demonstrates facile hydrolysis and strong polarity. It easily binds to polar water molecules and needs to overcome the larger dehydration resistance to pass through sub-nanochannels, which leads to its slower diffusion and lower ion flux. This substantial variation in migration rates significantly enhances the ion separation selectivity.

In addition, the hydrophilicity of the QA groups promotes the formation of a dual-phase structure within the membrane which increases the interaction with dehydrated ions[34]. To confirm the hydrophilic attributes of these groups, the water sorption characteristics within the membrane were investigated via dynamic vapor sorption curves (DVS) under varying relative humidity conditions (Fig. 6a). The findings indicate a slightly elevated water sorption rate in the QA-TB membrane compared to the TB membrane. However, the water sorption rate in both membranes remains low, not exceeding 20%, indicating that the membranes retain a considerable degree of hydrophobicity, as evidenced by their minimal swelling (Fig. 2c). The atomic force microscopy (AFM) results depicted in Fig. 6b-c clearly show that the TB membrane exhibits a uniform structure comprising solely hydrophobic polymer backbones. In contrast, the QA-TB membrane displays distinct light and dark regions due to the different hydrophilicity of the polymer and functional groups. The bright regions represent the hydrophobic segments of the polymer backbone, whereas the dark regions correspond to the hydrophilic portions of the quaternary ammonium groups[35]. The rigid and twisted structure of the TB polymer hampers the neat stacking of their main chain, resulting in a greater accumulation of hydrophobic skeletons in different directions and an increased hydrophobic area within the membrane. This structural arrangement creates ionized sub-nanochannels that enable dehydrated ions to rapidly migrate from these regions driven by an electric field[36]. To further explain the migration rates of different dehydrated anions within the ionized sub-nanochannels, the adsorption and desorption properties of $Cl^-/SO_4^{2-}/CO_3^{2-}$ along the polymeric backbone of QA-TB were analyzed by the density-functional theory (DFT)[37] calculation (Fig. 6d, Supplementary Figs. 14–15 and Supplementary Table 6). The adsorption and desorption of ions in the sub-nanochannels were attributed to the presence of electrostatic interaction forces between $Cl^-/SO_4^{2-}/CO_3^{2-}$ and the quaternary ammonium groups on the pore walls. The results show that dehydrated Cl^- has the lowest free energy, resulting in the shortest residence time and the fastest migration. This aligns well with the ultra-high selectivity between Cl^- and CO_3^{2-}/SO_4^{2-} in ionized QA-TB membranes.

Discussion

In summary, a quaternized TB microporous polymer membrane was prepared with exceptional separation selectivity for monovalent and divalent anions. The rigid V-shaped structure of the TB unit and the incorporation of specific QA groups construct ionized sub-nanochannels within the membrane, which optimize the size of the channels between the anion hydration diameter and their Stokes

diameter. Further investigation into the ion transport behavior with adsorption and desorption energies on the QA-TB framework revealed that the electrostatic interaction had a limited effect on Cl^- migration but greatly slowed the transfer of CO_3^{2-}, resulting in remarkable separation performance of monovalent and divalent anions. Overall, this research highlights opportunities to develop microporous polymer membranes for precise ion separation and provides a facile method to construct well-defined sub-nanochannels. These advancements may have broad applications in efficient, eco-friendly utilization of carbonate sources, water purification, and chemical separation.

Methods

Preparation of Anion Exchange Membranes (AEMs) and Cation Exchange Membranes (CEMs)

Here, 4 wt% TB/QA-TB microporous polymers and 2 wt% DOP were thoroughly dissolved in an NMP solution to prepare the casting solution. DOP was used to improve the flexibility of the membranes[38]. Subsequently, this solution was filtered through a 0.45 μm injection filter, and the filtrate was uniformly coated onto a glass plate. The phase inversion was performed at 60°C. Following the evaporation of the solvent, the glass plate was immersed in deionized water for the membrane to detach naturally. Similarly, 5 wt% SPEEK was dissolved in an NMP solution for the preparation of CEMs.

Membrane performance evaluation

Ion flux (J_i) and perm-selectivity (P). Ion separation experiments were performed in a laboratory-scale electrochemical device consisting of four compartments, a dilution chamber filled with a mixed salt solution of 0.1 mol L^{-1} NaCl and Na_2CO_3/Na_2SO_4, a concentration chamber containing a salt solution of 0.1 mol L^{-1} Na_2SO_4/Na_2CO_3, and two electrode chambers both circulating a 0.2 mol L^{-1} Na_2SO_4 solution. Each test assessed one anionic membrane and two cationic membranes, striking a balance between the concentration pressure difference of the system where the testing area of each membrane in the device spanned 19.63 cm^2. The ion concentrations of Cl^- and SO_4^{2-} were determined using ion chromatography (Shenghan CIC-D100, Qingdao), while the concentration of CO_3^{2-} was calculated using an acid-base titrator (Leici ZDJ-4B, Shanghai). The ion fluxes J_{Cl^-}, $J_{CO_3^{2-}}$, and $J_{SO_4^{2-}}$ of the membranes could be calculated by the following Eq. (1):

$$J_i = \frac{v\frac{dc_i}{dt}}{A} \tag{1}$$

where v is the volume of the dilution chamber solution (L), dt is the test time (s), dc_i is the concentration change of the target ion in the dilution chamber during the test time (mol L^{-1}), and A is the test area of the samples (m^2).

The perm-selectivity (P) of the membrane was calculated by the following Eq. (2):

$$P^{Cl^-}_{CO_3^{2-}/SO_4^{2-}} = \frac{J_{Cl^-} \cdot c_{CO_3^{2-}/SO_4^{2-}}}{c_{Cl^-} \cdot J_{CO_3^{2-}/SO_4^{2-}}} \tag{2}$$

where J_{Cl^-} and $J_{CO_3^{2-}/SO_4^{2-}}$ are the ion fluxes (mol m^{-2} s^{-1}), and c_{Cl^-} and $c_{CO_3^{2-}/SO_4^{2-}}$ are the ion concentrations in the dilution chamber (mol L^{-1}).

Data availability

All data supporting the findings of this study are available in the article, the Supplementary Information. Source Data including the coordinates of the optimized structures obtained by density functional theory calculation are provided via figshare (https://doi.org/10.6084/m9.figshare.25934497).

References

1. Wang, J., Tarhan, L. G., Jacobson, A. D., Oehlert, A. M. & Planavsky, N. J. The evolution of the marine carbonate factory. *Nature* **615**, 265–269 (2023).
2. Zhou, S. et al. Asymmetric pore windows in MOF membranes for natural gas valorization. *Nature* **606**, 706–712 (2022).
3. Wang, Z. et al. Electricity generation from carbon dioxide adsorption by spatially nanoconfined ion separation. *Nat. Commun.* **15**, 2672–2681 (2024).
4. Zuo, P. et al. Near-frictionless ion transport within triazine framework membranes. *Nature* **617**, 299–305 (2023).
5. Moss, A. B. et al. In operando investigations of oscillatory water and carbonate effects in MEA-based CO2 electrolysis devices. *Joule* **7**, 350–365 (2023).
6. He, M., Sun, Y. & Han, B. Green carbon science: efficient carbon resource processing, utilization, and recycling towards carbon neutrality. *Angew. Chem. Int. Ed. Engl.* **61**, 15–38 (2022).
7. Kamble, P. et al. A novel composite of monosodiumtitanate-amidoximatedpolyacrylonitrilefor the sequestration of uranium from contaminated water: an experimental and simulation study. *Sep. Purif. Technol.* **286**, 120477–120491 (2022).
8. Lu, M., Dong, J., Hu, M., Cheng, G. & Lv, J. Perovskite LaMnO3 composite graphene carbon nitride g-C3N4 improves the photocatalytic performance of tetracycline degradation. *Water* **15**, 1627–1643 (2023).
9. Liang, Y. et al. Polyamide nanofiltration membrane with highly uniform sub-nanometre pores for sub-1 A precision separation. *Nat. Commun.* **11**, 2015–2024 (2020).
10. Zhu, B. et al. Ultrapermeable gel membranes enabling superior carbon capture. *Chem. Int. Ed.* **63**, 1–8 (2023).
11. Chen, T. et al. Ultra-permeable zeolitic imidazolate frameworks-intercalated graphene oxide membranes for unprecedented ultrafast molecular separation. *Chem. Engin. J.* **419**, 129507–129519 (2021).
12. Goutham, S. et al. Beyond steric selectivity of ions using ångström-scale capillaries. *Nat. Nanotechnol.* **18**, 596–601 (2023).
13. Epsztein, R., DuChanois, R. M., Ritt, C. L., Noy, A. & Elimelech, M. Towards single-species selectivity of membranes with subnanometre pores. *Nat. Nanotechnol.* **15**, 426–436 (2020).
14. Jiang, Z. et al. Aligned macrocycle pores in ultrathin films for accurate molecular sieving. *Nature* **609**, 58–64 (2022).
15. Sheng, F. et al. Electro-nanofiltration membranes with positively charged polyamide layer for cations separation. *J. Membr. Sci.* **594**, 117453–117461 (2020).
16. Foglia, F. et al. Disentangling water, ion and polymer dynamics in an anion exchange membrane. *Nat. Mater.* **21**, 555–563 (2022).
17. Ban, T. et al. Efficient and durable vanadium flow batteries enabled by high-performance fluorinated poly(aryl piperidinium) membranes. *J. Mater. Chem. A.* **11**, 24013–24025 (2023).
18. Kim, S. & Lee, Y. M. Rigid and microporous polymers for gas separation membranes. *Prog. Polym. Sci.* **43**, 1–32 (2015).
19. Tan, R. et al. Hydrophilic microporous membranes for selective ion separation and flow-battery energy storage. *Nat. Mater.* **19**, 195–202 (2019).
20. Zhu, Q. et al. Solution-processable amorphous microporous polymers for membrane applications. *Prog. Polym. Sci.* **137**, 101636–101666 (2023).
21. Zhu, J. et al. Microporous organic polymer-based membranes for ultrafast molecular separations. *Prog. Polym. Sci.* **110**, 101308–101338 (2020).
22. Tang, Z. et al. Reaction site designation by intramolecular electric field in tröger's-base-derived conjugated microporous polymer for near-unity selectivity of CO2 photoconversion. *Adv. Mater.* **35**, 2210693–2210703 (2023).

23. Tang, H. et al. Fuel cells with an operational range of –20 °C to 200 °C enabled by phosphoric acid-doped intrinsically ultra-microporous membranes. *Nat. Energy* **7**, 153–162 (2022).
24. Carta, M. et al. Triptycene induced enhancement of membrane gas selectivity for microporous Tröger's base polymers. *Adv. Mater.* **26**, 3526–3531 (2014).
25. Zhu, Y. et al. Cation exchange membranes with bi-functional sites induced synergistic hydrophilic networks for selective proton transport. *Adv. Funct. Mater.* **33**, 2215109–2215119 (2023).
26. Yuan, W. et al. High performance poly(carbazolyl aryl piperidinium) anion exchange membranes for alkaline fuel cells. *J. Membr. Sci.* **657**, 120676–120685 (2022).
27. Sano, Y. & Nakashima, D. Prevention of calcium carbonate scale using electrolyzed water. *Int. J. Heat. Mass Tran.* **127**, 1147–1156 (2018).
28. Zhao, D., Xue, J., Li, S., Sun, H. & Zhang, Q.-d Theoretical analyses of thermal and economical aspects of multi-effect distillation desalination dealing with high-salinity wastewater. *Desalination* **273**, 292–298 (2011).
29. Pérez-González, A., Urtiaga, A. M., Ibáñez, R. & Ortiz, I. State of the art and review on the treatment technologies of water reverse osmosis concentrates. *Water Res.* **46**, 267–283 (2012).
30. Wang, P. et al. Construction of highly conductive PBI-based alloy membranes by incorporating PIMs with optimized molecular weights for high-temperature proton exchange membrane fuel cells. *J. Membr. Sci.* **659**, 120818–120827 (2022).
31. Zhang, K., Yu, W., Ge, X., Wu, L. & Xu, T. Molecular dynamics insight into phase separation and transport in anion-exchange membranes: effect of hydrophobicity of backbones. *J. Membr. Sci.* **661**, 120922–120934 (2022).
32. Huang, T. et al. Mechanically robust microporous anion exchange membranes with efficient anion conduction for fuel cells. *Chem. Eng. J.* **418**, 129311–129322 (2021).
33. Epsztein, R., Shaulsky, E., Dizge, N., Warsinger, D. M. & Elimelech, M. Role of ionic charge density in donnan exclusion of monovalent anions by nanofiltration. *Sci. Technol.* **52**, 4108–4116 (2018).
34. Zuo, P. et al. Ion exchange membranes: constructing and tuning ion ransport channels. *Adv. Funct. Mater.* **32**, 2207366–2207403 (2022).
35. Hu, C. et al. Multi-cation crosslinked anion exchange membranes from microporous Tröger's base copolymers. *J. Mater. Chem. A.* **6**, 13302–13311 (2018).
36. Li, R. et al. Electrodialysis for the volume reduction of the simulated radionuclides containing seawater. *J. Hazard. Mater.* **439**, 129601–129612 (2022).
37. Li Y. et al. Asymmetric coordination regulating d-orbital spin-electron filling in single-atom iron catalyst for efficient oxygen reduction. *Angew. Chem. Int. Ed.* **63**, e202405334 (2024).
38. Qin, Y. et al. New insights into tailoring polyamide structure for fabricating highly permeable reverse osmosis membranes. *Desalination* **499**, 114840–114852 (2021).

Acknowledgements

The authors acknowledge financial support from the National Natural Science Foundation of China (22208150, M.L.L.), Jiangsu Science and Technology Department (BZ2022012, BK20232010, S.P.S.), Jiangsu Future Membrane Technology Innovation Center (BM2021804, S.P.S. and M.L.L.), and the China Postdoctoral Science Foundation (2023M741664, M.L.L.). This work was partially supported by the Nano·Materials Technology Development program (RS–2023-00235295, Y.M.L.) through the (NRF) funded by the Ministry of Science and ICT of South Korea.

Author contributions

M.L.L. and Y.C. conceived the research, performed the polymer synthesis, membrane characterization, and performance test experiments, analyzed the data, and wrote the manuscript. C.H. and C.X.Z performed the characterization experiments. Z.J.F provided suggestions and guided the ion separation testing methods. Z.J.X. performed the density functional theory calculation. Y.M.L. and S.P.S. conceived the research, guided the project, edited the manuscript and supervised the work. All authors participated in the discussion and revised the manuscript.

Competing interests

The authors declare no competing interests.

Additional information

Supplementary information The online version contains supplementary material available at https://doi.org/10.1038/s41467-024-51540-1.

Correspondence and requests for materials should be addressed to Young Moo Lee or Shi-Peng Sun.

Peer review information *Nature Communications* thanks the anonymous reviewers for their contribution to the peer review of this work. A peer review file is available.